EarthArXiv Preprint Notice

Title:
Forward-Only Temporal-Coherence Occupancy Regimes in Atlantic Tropical Cyclone Intensity Evolution (1851–2024)

Author:
Nathan Howell
PTEM Labs LLC

Preprint Status:
This manuscript is a non-peer-reviewed preprint submitted to EarthArXiv.

Journal Submission Status:
Currently under review / resubmitted to *Weather and Forecasting* (American Meteorological Society).

Version Notice:
This version supersedes prior preprint versions and includes expanded methodological formalization, revised interpretive framing, additional sensitivity analyses, and updated reproducibility materials.

Forward-Only Temporal-Coherence Occupancy Regimes in Atlantic Tropical Cyclone Intensity Evolution (1851–2024)

Nathan Howell
PTEM Labs, Atlantic Beach, Florida, USA
ORCID: 0009-0009-8893-6260
Corresponding author: nate@ptemlabs.com

Abstract

Rapid intensification (RI) remains one of the most consequential and difficult-to-characterize aspects of tropical cyclone intensity evolution, commonly defined as an increase in maximum sustained wind speed of at least 30 kt within 24 h (Kaplan and DeMaria 2003; Kaplan et al. 2010; DeMaria et al. 2021). This study evaluates whether Atlantic best-track intensity records contain forward-detectable temporal occupancy regimes. A minimal diagnostic is constructed from HURDAT2 using causal rolling means of maximum sustained wind speed across multiple advisory-window lengths and a directional-agreement activation rule. The framework is evaluated under replay-constrained execution and frozen parameter governance using only current and prior intensity values from 1,991 Atlantic tropical cyclones during 1851–2024.

Storms occupying the active regime for longer cumulative durations form a subset with elevated conditional RI occurrence. Conditional RI occurrence increases from a basin-wide baseline of approximately 26% to about 60% for storms with at least 140 h of active occupancy and to about 67% for storms with at least 168–270 h of active occupancy. Diagnostic behavior is additionally characterized using occupancy climatology, lifecycle-relative onset structure, and lead-time survival analysis. Alignment significance is evaluated against autocorrelated block-shuffle and phase-constrained null frameworks designed to preserve storm lifecycle evolution.

Occupancy behavior remained stable across parameter neighborhoods, preserved timing organization under constrained null frameworks, and retained separable timing structure under tested conditioned formulations, although advisory-level occupancy coefficients attenuated substantially in shared-sample models. These results support interpretation of the diagnostic as a

forward-only occupancy framework for temporal organization in tropical cyclone intensity evolution.

1. Introduction

Rapid intensification (RI), typically defined as an increase in maximum sustained wind speed of at least 30 kt within 24 h, remains one of the most consequential and difficult-to-forecast aspects of tropical cyclone evolution (Kaplan and DeMaria 2003; Kaplan et al. 2010; DeMaria et al. 2021). Despite advances in statistical-dynamical guidance and environmental diagnostics, RI remains difficult to characterize, and storms embedded in broadly favorable environments can still follow different intensity-evolution pathways. Prior work has established the importance of environmental conditions such as vertical wind shear, sea surface temperature, and ocean heat content, and persistence terms are already embedded in operational and statistical RI guidance (Kaplan and DeMaria 2003; Kaplan et al. 2010; DeMaria et al. 2021). However, recent intensity change, storm duration, and fixed-threshold RI labels capture related but not identical aspects of intensity evolution; here we test whether a simple multi-window directional-agreement diagnostic provides additional stratification beyond those baselines within the Atlantic archive (Torrence and Compo 1998; Ng and Chan 2012; Theiler et al. 1992). This distinction motivates a descriptive long-record analysis of whether cross-scale agreement regimes can be identified in best-track intensity evolution. Temporal coherence is defined here operationally as sustained directional agreement among causal rolling-mean representations of the same intensity-evolution record across multiple temporal windows.

Structure-resolving observations are largely confined to the satellite and aircraft reconnaissance eras. Best-track intensity records provide much longer temporal coverage than structure-resolving observations from aircraft, microwave, radar, or other satellite products. HURDAT2 therefore supports long-record analysis of intensity evolution, but it contains limited direct information about inner-core structure and is not sufficient by itself to diagnose convective organization, vortex alignment, or physical mechanism (Landsea and Franklin 2013; Landsea et al. 2022; Vecchi and Knutson 2008, 2011). This motivates a narrower descriptive question: do Atlantic best-track intensity records contain forward-detectable temporal coherence regimes, and

does longer occupancy of those regimes correspond to redistributed conditional RI occurrence? The focus is regime characterization first; RI is used as an outcome layer for evaluating whether the detected regimes distinguish meaningful storm behavior.

This study defines the detector, characterizes occupancy climatology, evaluates RI occurrence conditional on occupancy duration, and tests reduction to simpler persistence and duration baselines. The method is intentionally minimal and reproducible. Occupancy was evaluated using survival-style timing analysis, parameter-stability surfaces, autocorrelation-preserving null frameworks, and environmental conditioning experiments (Kaplan and Meier 1958; Cox 1972; Andersen and Gill 1982; Allison 1982).

The framework is evaluated as a temporal-occupancy instrument. Activation states use strict forward-only constraints, fixed parameter governance, and frozen replay conditions; event alignment is assessed through occupancy duration, event-time behavior, and survival-style timing analysis.

---

2. Data

This analysis uses the Atlantic hurricane database HURDAT2 (Landsea et al. 2022), which contains best-track information for 1,991 tropical cyclones spanning 1851–2024. For each storm and advisory time, the dataset provides storm position and maximum sustained wind speed (VMAX). In this study, VMAX is used to construct the temporal-coherence diagnostic and to define RI events. Rapid intensification is defined as an increase in VMAX of at least 30 kt over 24 h, consistent with established operational and research conventions (Kaplan and DeMaria 2003; Kaplan et al. 2010; DeMaria et al. 2021).

HURDAT2 is not temporally homogeneous across the full record. Earlier portions of the dataset are subject to greater uncertainty in storm detection and intensity estimation, particularly prior to the aircraft and satellite eras (Landsea and Franklin 2013; Vecchi and Knutson 2008, 2011; Vecchi et al. 2021). The goal is to evaluate whether a causal multi-window alignment property can be characterized across the archive despite these known constraints. Records that do not support the required current-and-prior rolling-window calculation are excluded from that time

step rather than filled using future information. These limitations are considered in interpretation but are not explicitly corrected in the present analysis.

3. Causal temporal-coherence detector

3.1. Temporal-coherence diagnostic

Let $V(t)$ denote maximum sustained wind speed at advisory time t. For each storm, causal rolling means are computed over $s \in \{3,5,9\}$ advisory windows:

$$\bar{V}_s(t) = \frac{1}{s}\sum_{k=0}^{s-1} V\,(t-k), \qquad s \in \{3,5,9\}.$$

These correspond to approximately 18-, 30-, and 54-h windows under 6-h advisory spacing. Each rolling mean uses only the current and prior observations.

For each smoothed series, a one-step tendency is defined as:

$$D_s(t) = \bar{V}_s(t) - \bar{V}_s(t-1), \qquad s \in \{3,5,9\}.$$

Directional agreement is evaluated across the three window pairs $(3,5)$, $(5,9)$, and $(3,9)$:

$$A_{ij}(t) = \begin{cases} 1, & \text{if } \operatorname{sign}\big(D_i(t)\big) = \operatorname{sign}\left(D_j(t)\right), \\ 0, & \text{otherwise,} \end{cases} \qquad (i,j) \in \{(3,5),(5,9),(3,9)\}.$$

The agreement score is:

$$PL(t) = \frac{1}{3}\sum_{(i,j)\in\mathcal{P}} A_{ij}\,(t), \qquad \mathcal{P} = \{(3,5),(5,9),(3,9)\}.$$

Because sign equality is transitive, the three pairwise comparisons are not interpreted as independent dimensions. The score is used operationally to classify whether the smoothed tendencies occupy a common directional state under forward-only replay.

3.2. Activation rule and occupancy

A time step is classified as active when:

$$\mathrm{PL}(t) \geq 0.67$$

and this condition is sustained for at least two consecutive advisories. Since $\mathrm{PL}(t)$ can take values 0, $1/3$, $2/3$, and 1, the threshold 0.67 is the minimum value indicating agreement among at least two of the three pairwise comparisons. Under the three-window construction, sustained activation identifies intervals in which the smoothed tendencies occupy a common directional state.

For each storm, active occupancy duration is defined as:

$$I_{\mathrm{active}}(t) = \mathbf{1}\{t\ extisactiveundertheruleabove\},$$

$$O = 6\sum_{t} I_{\mathrm{active}}\,(t),$$

where O is measured in hours and $\mathbf{1}\{\cdot\}$ is the indicator function. A continuous sequence of active advisories is defined as an occupancy episode. The first active advisory in an episode is the episode onset, and the first subsequent inactive advisory marks episode termination.

Primary enrichment statistics are summarized at the storm level to avoid treating within-storm advisory times as independent samples. Analyses involving timing or duration are treated explicitly as occupancy-process analyses.

The primary detector configuration and RI endpoint definition used throughout the analysis are summarized in Table 1.

Table 1. Causal detector parameterization and RI endpoint definition.

Parameter	Value	Interpretation
Cadence	6 h	Advisory sampling interval for detector updates.
Windows	3,5,9 advisories / 18,30,54 h	Multi-window alignment used for coherence scoring.
Activation threshold	PL >= 0.67	Active state defined when PL ≥ 0.67.
Minimum occupancy duration	2 advisories	Requires at least 12 h of consecutive activation at 6 h cadence.
Input	VMAX only	Detector built only from best-track intensity evolution.
Computation	forward-only current/prior observations	No look-ahead features; only current and historical values at each advisory.
RI threshold	>=30 kt / 24 h	Rapid intensification outcome definition.

3.3. Interpretation

The diagnostic is observational. It identifies sustained cross-timescale directional agreement in best-track intensity evolution under causal constraints, without directly measuring storm evolution, environmental favorability, or causality.

3.4. Baseline comparison metrics

To evaluate whether occupancy adds information beyond simpler persistence constructions, baseline comparison metrics were constructed. Single-window persistence metrics were computed separately using 3-, 5-, and 9-advisory causal rolling means, with activity defined when the one-step tendency remained positive for at least two consecutive advisories. Additional baseline metrics include storm duration, recent 24-h intensity change, recent 48-h intensity change, and storm-level mean intensification rate. These comparisons test whether active occupancy provides stratification beyond simpler measures of intensification persistence and storm longevity.

4. Occupancy climatology, event-time structure, and RI stratification

4.1. Occupancy climatology

To characterize the temporal behavior of the framework beyond storm-level enrichment statistics, activation episodes were analyzed as occupancy processes evolving through normalized tropical cyclone lifecycle space. Diagnostics included occupancy prevalence, episode duration patterning, lifecycle-relative timing distributions, and occupancy-phase climatology. These analyses tested whether activations formed temporally clustered active intervals instead of isolated threshold exceedances.

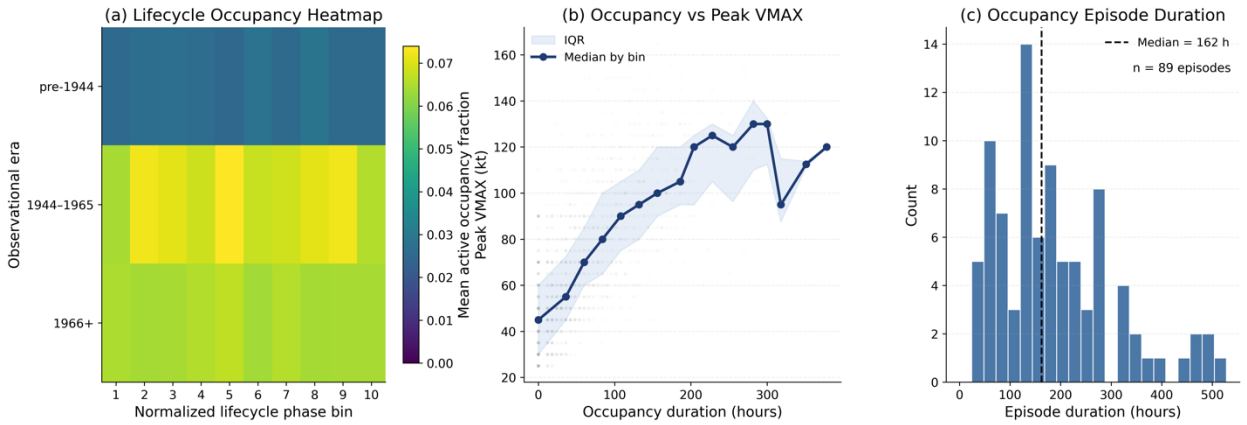

Figure 1 summarizes occupancy climatology diagnostics, including lifecycle-relative occupancy prevalence (Fig. 1a), occupancy duration versus peak intensity (Fig. 1b), and occupancy-episode duration patterning (Fig. 1c).

Figure 1a shows lifecycle-relative occupancy prevalence across normalized storm evolution, stratified by observational era. Figure 1b summarizes the relationship between occupancy duration and storm peak intensity, including median alignment and interquartile spread across occupancy bins. Figure 1c shows the distribution of occupancy-episode durations across the Atlantic archive, illustrating the sparse upper-tail behavior of long-duration active episodes.

Occupancy was not uniformly distributed across storm evolution. Instead, activation prevalence concentrated within preferred lifecycle intervals, indicating that the framework preferentially identifies structured temporal regimes rather than isolated or randomly dispersed intensity fluctuations. This concentration supports interpretation of the detector as an event-time occupancy framework, not merely a threshold exceedance classifier.

Occupancy duration varied substantially across storms. Extended active intervals were relatively uncommon and clustered disproportionately among higher-intensity outcomes, whereas short-duration occupancy occurred broadly across the basin climatology. This patterning suggests that upper-tail occupancy behavior represents a distinct temporal regime rather than a uniform amplification across all storms.

Active episodes were not uniformly long-lived. Most episodes occupied the lower-to-intermediate duration range, while a sparse upper tail extended to several hundred hours. This supports treating activation episodes as temporally bounded intervals rather than as a continuously active storm classification.

4.2. Event-time structure

Because activation episodes evolve through time rather than occurring as isolated classifications, event alignment was evaluated explicitly using lead-time distributions, onset-offset configuration, survival-style diagnostics, and autocorrelation-preserving null comparisons.

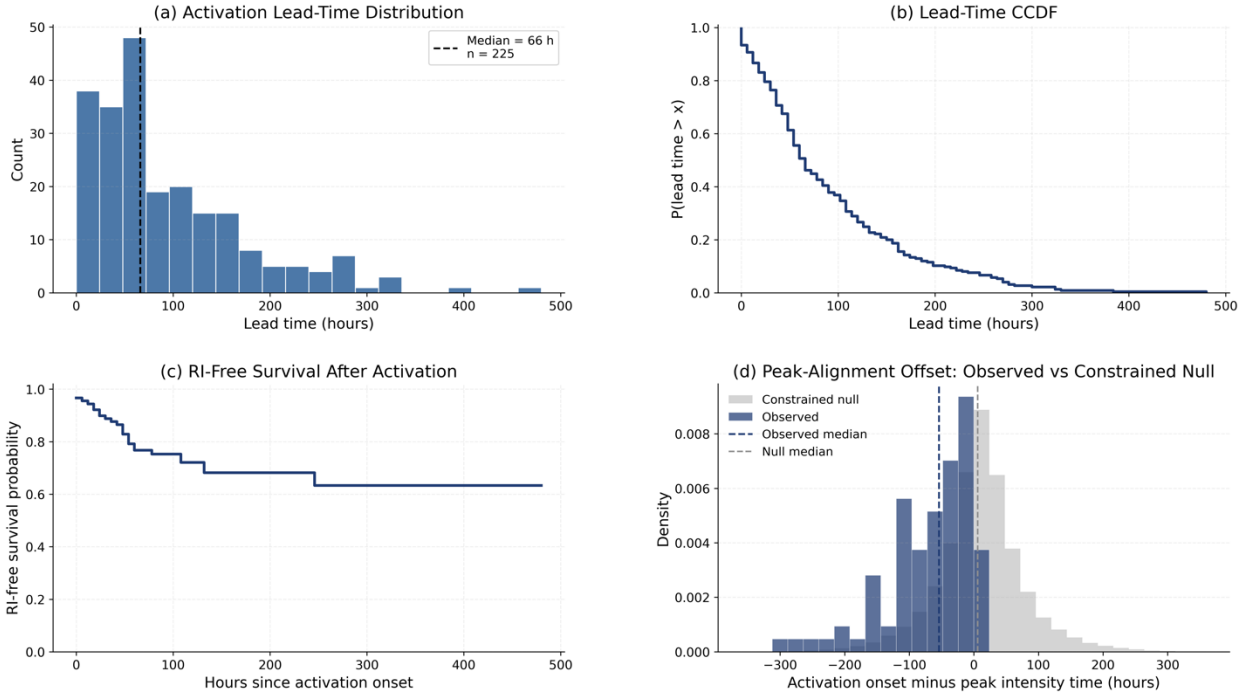

Figure 2. Event-time structure of temporal-coherence occupancy episodes. (a) Distribution of activation lead times relative to downstream lifecycle milestones. (b) Complementary cumulative distribution function (CCDF) of activation lead times, highlighting upper-tail advance timing behavior. (c) RI-free survival following activation onset. (d) Observed onset-alignment density compared with constrained-null realizations preserving lifecycle occupancy structure.

Figure 2a shows the distribution of activation lead times relative to downstream lifecycle milestones. Figure 2b presents the complementary cumulative distribution function (CCDF) of lead times, highlighting upper-tail advance timing behavior. Figure 2c shows RI-free survival following activation onset. Figure 2d compares observed onset-alignment configuration against constrained null realizations preserving different components of temporal organization.

Lead times exhibited substantial dispersion but were strongly skewed toward positive advance alignment, with most activations occurring prior to major lifecycle milestones. The resulting distribution was heavy-tailed rather than sharply peaked, indicating that activation episodes do not occur at a single preferred lead horizon.
The gradual CCDF decay indicates that activation episodes can occur well before downstream lifecycle transitions. This upper-tail lead patterning is not fully reproduced by local-fluctuation behavior alone and motivates the dependence-aware controls evaluated here. (Theiler et al. 1992; Künsch 1989; Politis and Romano 1994).

Observed onset distributions were systematically shifted toward earlier alignment relative to autocorrelation-preserving null realizations. Although the null frameworks preserve substantial lifecycle evolution, the empirical activations retained distinct timing organization not reproduced under randomized temporal alignment.

Similar alignment behavior was observed relative to hurricane attainment milestones, indicating that the timing behavior was not confined solely to peak-intensity alignment.

4.3. RI stratification

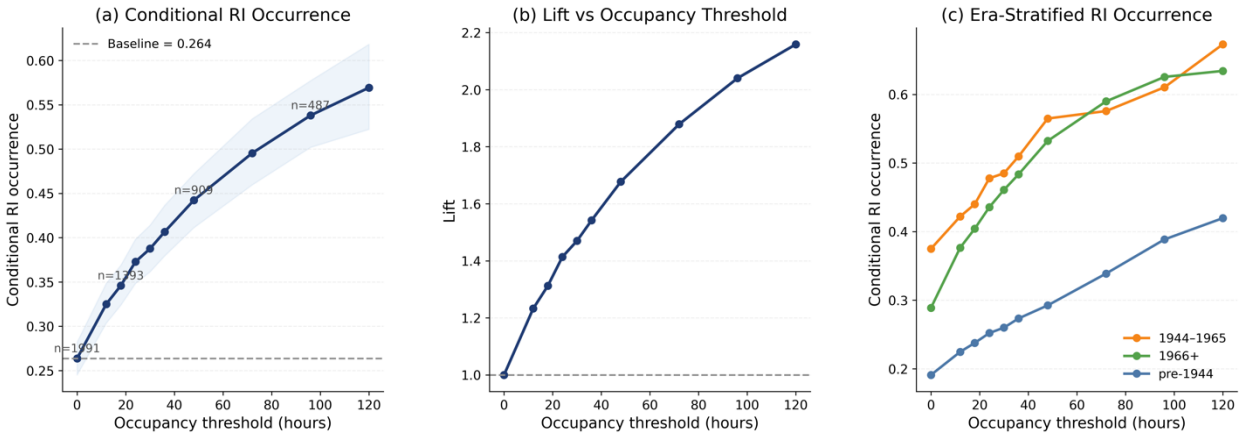

Figure 3. Occupancy-conditioned rapid-intensification stratification across the Atlantic record.

(a) Conditional RI occurrence as a function of cumulative active duration. Error bars indicate 95% bootstrap confidence intervals and sample sizes are annotated at representative thresholds. (b) RI lift relative to the basin baseline as a function of occupancy duration threshold. (c) Era-stratified conditional RI occurrence curves for pre-1944, mid-century, and modern observational subsets. Upper-tail estimates are sample-limited and should be read in light of known historical observing-system inhomogeneities. (Landsea and Franklin 2013; Vecchi and Knutson 2008, 2011).

The occupancy–RI relationship exhibits progressive enrichment across increasing occupancy-duration thresholds, with longer active occupancy associated with elevated conditional RI occurrence. Uncertainty increases in upper-tail occupancy cohorts as sample size declines, but monotonic enrichment remains visible across observational eras. The framework therefore identifies a conditionally enriched occupancy regime rather than a deterministic RI classification boundary.

Storms occupying the active alignment regime for longer cumulative durations formed a progressively smaller subset with elevated conditional RI occurrence. Across the Atlantic dataset (1851–2024; 1,991 storms), 525 storms satisfy the rapid intensification (RI) definition,

corresponding to a basin-wide conditional RI occurrence of approximately 26.4%. Storms stratified by active duration exhibit a largely monotonic increase in conditional RI occurrence. For storms with at least 72 h of active occupancy, RI occurrence increases to approximately 49.6% (n = 659). At higher occupancy thresholds, enrichment continues: 60.1% for ≥140 h (n = 228), 66.4% for ≥168 h (n = 146), and 66.7% for ≥270 h (n = 24). Observational-era stratification shows similar enrichment at low-to-intermediate occupancy thresholds, although upper-tail estimates become unstable in some eras because of small sample sizes (Fig. 3c). Differences in absolute RI occurrence across eras are consistent with known observational and intensity-estimation changes. These results support long-record robustness across the tested strata, while not establishing full observing-system independence.

RI occurrence statistics across representative duration thresholds are summarized in Table 2.

Table 2. Conditional RI occurrence and enrichment across occupancy-duration thresholds.

threshold	n_storms	n_ri	conditional_ri_occurrence	lift	bootstrap_low	bootstrap_high
0.0	1991	525	0.264	1.000	0.245	0.282
12.0	1526	496	0.325	1.233	0.304	0.349
18.0	1393	482	0.346	1.312	0.324	0.369
24.0	1258	469	0.373	1.414	0.348	0.398
30.0	1179	457	0.388	1.470	0.362	0.414
36.0	1087	442	0.407	1.542	0.379	0.436
48.0	909	402	0.442	1.677	0.411	0.472
72.0	658	326	0.495	1.879	0.460	0.534
96.0	487	262	0.538	2.040	0.502	0.577
120.0	339	193	0.569	2.159	0.522	0.618

Stratification by observational era shows that the occupancy–RI relationship is preserved across multiple historical regimes (Fig. 3c), with similar monotonic structure evident in pre-1944, mid-century, and modern subsets. Differences in absolute RI probability across eras are consistent with known observational and intensity estimation differences, but the underlying relationship

remains intact.

Bootstrap confidence intervals indicate that enrichment remains distinct from the basin baseline across low-to-intermediate thresholds up to at least 168 h. At higher thresholds, uncertainty widens sharply because of reduced sample size, and those estimates are treated as exploratory. The diagnostic therefore identifies a conditionally enriched occupancy regime rather than broadly detecting all RI events. The observed pattern is best interpreted as evidence that persistent occupancy alignment stratifies RI occurrence within the historical record.

---

5. Reduction, robustness, and sensitivity analyses

5.1. Parameter stability surfaces

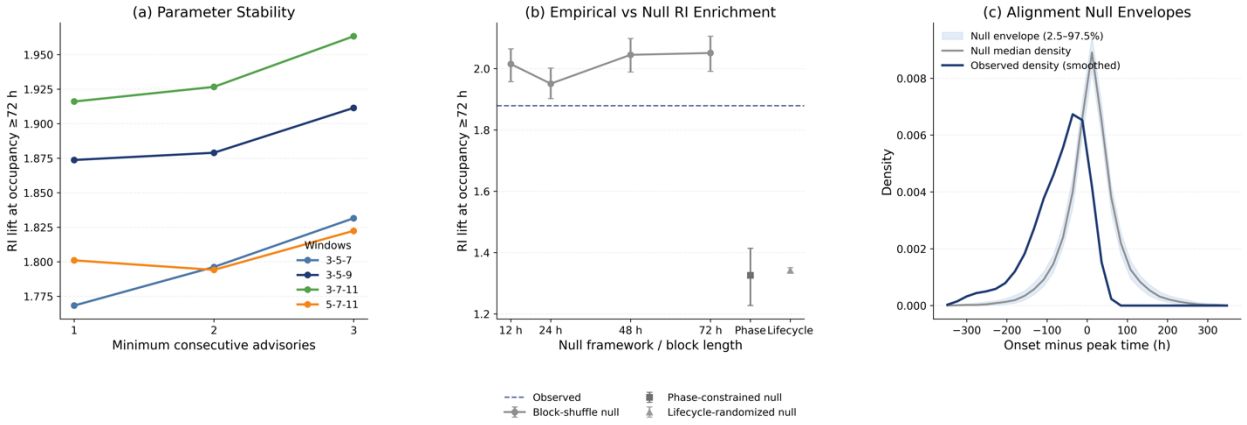

Figure 4. Parameter sensitivity and constrained-null comparisons for the temporal-coherence occupancy framework. (a) RI lift at occupancy ≥72 h across alternative smoothing-window triplets and minimum consecutive-advisory requirements. (b) Empirical RI enrichment compared with constrained null frameworks preserving different components of temporal organization. Phase-constrained and lifecycle-randomized nulls yield weaker enrichment than observed, whereas block-shuffle nulls retain partial enrichment after autocorrelation-preserving temporal reordering. (c) Observed onset-alignment density relative to constrained null envelopes; shading indicates the 2.5–97.5% null envelope and the gray curve indicates the null median density.

Diagnostic behavior was stable across the tested parameter neighborhood, with RI enrichment at occupancy ≥72 h remaining positive across alternative smoothing-window triplets and persistence requirements. The constrained-null comparisons indicate that part of the occupancy–RI relationship is expected from autocorrelated intensity evolution, especially under block-shuffle controls. However, phase-constrained and lifecycle-randomized nulls produce weaker enrichment, and the onset-alignment envelope shows earlier empirical timing than the constrained-null median. These results show dependence on autocorrelated intensity evolution, while retaining event-time organization not reproduced by the simpler constrained timing controls.

5.2 Null frameworks

Multiple null frameworks were constructed to evaluate whether the observed occupancy–RI relationship could be reproduced through autocorrelation, lifecycle evolution, or randomized alignment alone. Phase-preserving and lifecycle-randomized null constructions produced substantially weaker enrichment than the empirical framework. Autocorrelation-preserving block-shuffle nulls retained enrichment, indicating that temporal dependence contributes materially to the observed relationship.

Representative enrichment behavior across the primary constrained null-framework families is summarized in Table 3.

Table 3. Null-framework comparison of RI enrichment at occupancy ≥72 h.

framework	preserved_structure	disrupted_structure	observed_lift_ge_72h	null_lift_ge_72h	interpretation
block_shuffle	Intra-storm autocorrelation and marginal intensity distribution within shuffled blocks	Long-range temporal ordering across blocks	1.879	2.051	Block-shuffle null retained partial enrichment under constrained temporal reordering
phase_preserving	Activation constrained to	Exact activation onset timing and	1.879	1.326	Phase-constrained null mean lift is

	genesis-to-peak phase envelope with storm-level activity retained	event-specific sequencing			below observed lift.
lifecycle_randomized	Storm-level active duration with randomized onset within lifecycle phase bins	Observed onset placement and timing alignment	1.879	1.342	Lifecycle-randomized null mean lift is below observed lift.

The strongest autocorrelation-preserving null frameworks retained partial enrichment behavior, indicating that some occupancy–RI association is expected from the autocorrelated organization of intensity evolution itself. Because intensity evolution is autocorrelated, the relevant test is not complete null collapse; it is whether empirical timing and alignment remain separable under constrained temporal controls.

Null-aligned timing envelopes further demonstrated that empirical activation timing retained coherent advance patterning relative to both phase-preserving and lifecycle-randomized controls. The observed timing organization therefore cannot be explained solely through randomized lifecycle occupancy placement.

A block-shuffle null was constructed by shuffling intensity-evolution blocks of length 12-, 24-, and 48-h within storms. This disrupts temporal ordering while preserving portions of within-storm intensity evolution. Under block shuffling, the relationship was attenuated but not eliminated. Thus, the occupancy signal depends partly on autocorrelated intensity evolution, while empirical timing preserved alignment differences under several constrained null constructions.

5.3. Bootstrap uncertainty

Uncertainty in the occupancy-conditioned RI relationship was evaluated using storm-level bootstrap resampling. Across all occupancy thresholds, bootstrap confidence intervals remain well above the basin baseline, indicating that the observed enrichment is not driven by sampling

variability (Efron 1979; Efron 1986). While uncertainty increases in the highest-occupancy cohorts due to small sample size, the central tendency of the relationship remains stable.

5.4 Environmental overlap and conditioning

Environmental-conditioning analyses were performed on a shared advisory-level sample under strict causal constraints, duplicate-row removal, post-event truncation, and cluster-aware inference safeguards. Environmental covariates retained meaningful explanatory behavior after occupancy inclusion, while storm-level occupancy aggregates retained positive conditioned coefficients under the tested storm-level formulations. These analyses test whether occupancy behavior remains distinguishable after environmental conditioning; they do not establish causal independence from the environmental covariates. Summary statistics from the shared-sample environmental-conditioning audit are provided in Table 4 (Liang and Zeger 1986; Lin and Wei 1989; Andersen and Gill 1982).

Table 4. Environmental conditioning audit summary under shared-sample, causal constraints.

model	sample	covariates	occupancy coefficient	attenuation relative to unconditioned	AIC or ΔAIC	interpretation
A. Occupancy only (shared advisory)	5667 rows / 422 storms / 135 events	cumulative_occupancy_hours_scaled (+ storm_age_hours, vmax, active)	0.181	0%	AIC 1251.9	Baseline occupancy term on shared sample;
B. Environmental only (shared advisory)	5667 rows / 422 storms / 135 events	env_U200, env_RHMD, env_DSST, env_NOHC, env_Z850, env_D200 (+ storm_age_hours, vmax)		NA	AIC 1207.1	Environmental baseline for ΔAIC and occupancy-conditioning comparisons.
C. Occupancy + environmental (shared advisory)	5667 rows / 422 storms / 135 events	Model B + cumulative_occupancy_hours_scaled	-0.046	125%	ΔAIC vs B 1.8	Comparable attenuation estimate; coefficient sign reversal
D. Occupancy + duration + environmental (storm-level)	422 storms / 135 event storms	env means + duration_hours + total_occupancy_hours_scaled + max_active_run_hours_scaled	1.431	NA (no same-sample storm-level unconditioned occupancy model)	ΔAIC vs storm env-only -4.4	Positive storm-level occupancy aggregate; unit review required for direct manuscript scaling note.

Across the shared-sample advisory conditioning experiments, occupancy-duration terms attenuated substantially after inclusion of the tested environmental covariates. In the directly comparable shared-sample advisory specification, the occupancy coefficient changed from 0.181 (OR 1.199) in the occupancy-only model to -0.046 (OR 0.955) after environmental covariate inclusion, corresponding to substantial attenuation of the advisory-level occupancy relationship. However, storm-level occupancy aggregates remained positively associated with RI occurrence under conditioned formulations. These analyses are interpreted as descriptive reduction tests rather than evidence of causal independence or operational forecast superiority. The advisory-level attenuation therefore constrains interpretation of the public VMAX-only occupancy diagnostic as an environmentally independent predictor. Because the advisory-level and storm-level formulations operate on different aggregation configurations and dependence assumptions, their coefficients are not directly comparable.

5.5. Failure topology

The framework does not identify all RI events and is not equivalent to a generic intensification detector.

Table 5. Failure-topology cohort definitions and counts.

topology_class	definition	count	interpretation
active_plus_no_ri	active_any=1 and ri_flag=0	1030	Activated storms without RI are the largest cohort.
active_plus_ri	active_any=1 and ri_flag=1	496	Activated storms that realize RI.
inactive_plus_no_ri	active_any=0 and ri_flag=0	436	Inactive storms that do not realize RI.
high_occupancy_no_ri	occupancy_hours>=72 and ri_flag=0	332	Long occupancy does not guarantee RI realization.
long_coherent_weak	occupancy_hours>=72 and peak_vmax<64	74	Sustained coherence can occur in storms that remain below hurricane strength.
ri_low_occupancy	ri_flag=1 and occupancy_hours<24	56	RI can occur with low pre-RI occupancy.
abrupt_ri	ri_flag=1 and occupancy_hours<24	56	Operationally equivalent to ri_low_occupancy in current implementation.
inactive_plus_ri	active_any=0 and ri_flag=1	29	RI events missed by activation logic.

Failure-topology cohorts were evaluated to characterize the dominant activation and non-activation outcome patterning. Cohort definitions and storm counts are summarized in Table 5.

5.6. Sensitivity to parameter choices

Sensitivity was evaluated across alternative rolling-window triplets ((3,5,7), (3,5,9), (3,7,11), and (5,7,11)), activation thresholds (0.5, 0.67, and 1.0), and consecutive-advisory occupancy requirements (1–3 advisories). For each configuration, RI occurrence, sample size, confidence intervals, and lift relative to the basin baseline were recomputed. Results are reported in Table 6.

Table 6. Sensitivity analysis across alternative smoothing-window triplets, activation thresholds, and minimum consecutive-advisory requirements. Reported metrics include conditional RI occurrence at occupancy ≥72 h, RI lift relative to the basin baseline, activation prevalence, and median occupancy duration.

windows	threshold	min_consecutive	ri_occurrence_ge_72h	lift_ge_72h	activation_prevalence	median_occupancy_hours
3,5,7	0.5	1	0.466	1.768	0.904	54.0
3,5,7	0.5	2	0.474	1.796	0.838	54.0
3,5,7	0.5	3	0.483	1.831	0.779	48.0
3,5,7	0.67	1	0.466	1.768	0.904	54.0
3,5,7	0.67	2	0.474	1.796	0.838	54.0
3,5,7	0.67	3	0.483	1.831	0.779	48.0
3,5,7	1	1	0.466	1.768	0.904	54.0
3,5,7	1	2	0.474	1.796	0.838	54.0
3,5,7	1	3	0.483	1.831	0.779	48.0
3,5,9	0.5	1	0.494	1.874	0.839	42.0
3,5,9	0.5	2	0.495	1.879	0.766	36.0
3,5,9	0.5	3	0.504	1.911	0.694	36.0
3,5,9	0.67	1	0.494	1.874	0.839	42.0
3,5,9	0.67	2	0.495	1.879	0.766	36.0
3,5,9	0.67	3	0.504	1.911	0.694	36.0
3,5,9	1	1	0.494	1.874	0.839	42.0
3,5,9	1	2	0.495	1.879	0.766	36.0

3,5,9	1	3	0.504	1.911	0.694	36.0
3,7,11	0.5	1	0.505	1.916	0.763	30.0
3,7,11	0.5	2	0.508	1.927	0.687	30.0
3,7,11	0.5	3	0.518	1.963	0.619	24.0
3,7,11	0.67	1	0.505	1.916	0.763	30.0
3,7,11	0.67	2	0.508	1.927	0.687	30.0
3,7,11	0.67	3	0.518	1.963	0.619	24.0
3,7,11	1	1	0.505	1.916	0.763	30.0
3,7,11	1	2	0.508	1.927	0.687	30.0
3,7,11	1	3	0.518	1.963	0.619	24.0
5,7,11	0.5	1	0.475	1.801	0.785	42.0
5,7,11	0.5	2	0.473	1.794	0.715	36.0
5,7,11	0.5	3	0.481	1.822	0.654	36.0
5,7,11	0.67	1	0.475	1.801	0.785	42.0
5,7,11	0.67	2	0.473	1.794	0.715	36.0
5,7,11	0.67	3	0.481	1.822	0.654	36.0
5,7,11	1	1	0.475	1.801	0.785	42.0
5,7,11	1	2	0.473	1.794	0.715	36.0
5,7,11	1	3	0.481	1.822	0.654	36.0

Because the three-window construction yields discrete agreement states (0, 1/3, 2/3, 1), the 0.67 and 1.0 thresholds produce similar activation behavior after persistence filtering, with both preferentially retaining sustained full-agreement states.

5.7. Observational era stratification

The dataset was partitioned into observational eras to evaluate whether RI enrichment conditioned on occupancy duration is confined to a particular observing regime. Enrichment is present at low-to-intermediate occupancy thresholds across eras, but upper-tail estimates are sensitive to small sample sizes. The persistence of low-to-intermediate-threshold enrichment across observational eras indicates that the occupancy–RI relationship is not confined to a single observing regime, although upper-tail estimates remain sensitive to sparse historical sampling.

5.8. Duration normalization

To evaluate whether active occupancy simply reflects storm longevity, analyses were repeated using duration-normalized occupancy and stratification within storm-lifetime bins. The occupancy–conditioned RI relationship remained positive under duration normalization, although effect sizes were reduced relative to the unnormalized threshold analysis. Storm lifetime contributes to the stratification but does not fully account for it.

5.9. Logistic regression analysis

Logistic regression models were constructed to evaluate whether active duration provides explanatory information beyond storm duration and simpler intensity-evolution summaries. In a univariate model, occupancy duration exhibits a positive coefficient. When storm duration is included as a covariate, the occupancy coefficient remains positive, while the duration contribution is reduced. Model fit statistics, including log-likelihood, AIC, and pseudo-$\boldsymbol{R^2}$, are reported in Table 7. Effect sizes are interpreted cautiously; the regression is used to test reduction to simpler covariates, not to propose an operational forecast equation. Occupancy-duration terms retained explanatory contribution under joint modeling configurations, supporting the interpretation that the detector captures organized temporal occupancy behavior beyond gross storm duration alone.

Table 7. Logistic regression comparison of occupancy duration and duration-controlled RI models.

model	occupancy_coef	occupancy_p	duration_coef	duration_p	AIC	R^2	n_storms
occupancy only	0.015	<0.001	NA	NA	1985.519	0.137	1991
duration only	NA	NA	0.008	<0.001	2036.222	0.115	1991
occupancy plus duration	0.015	<0.001	0.0	0.961	1987.516	0.137	1991
single window plus duration	0.01	<0.001	0.004	<0.001	2015.272	0.125	1991

5.10. Comparison with single-window persistence metrics

Single-window comparators based on the 3-, 5-, and 9-advisory rolling means also exhibit positive association with RI occurrence, confirming that event-time organization contains

meaningful information. However, the multi-window occupancy diagnostic provides more stable stratification across intermediate occupancy thresholds and is less sensitive to any single smoothing scale. The comparison therefore suggests that directional agreement across multiple rolling-window representations sharpens occupancy stratification relative to single-window persistence alone (Torrence and Compo 1998; Ng and Chan 2012).

At higher alignment regime thresholds, the single-window persistence comparator becomes unstable due to small sample sizes, with sharp fluctuations in estimated conditional RI occurrence. In contrast, the multi-window diagnostic maintains a more consistent upper-tail behavior, indicating improved discrimination of persistent storm evolution.

Logistic regression results further support this distinction. While the single-window persistence metric is positively associated with RI occurrence, its effect weakens when controlling for storm duration. In contrast, the multi-window temporal-coherence metric retains a stronger and more stable relationship with RI under duration control, indicating that it retains association after accounting for storm longevity under the tested model configurations.

These results indicate that temporal coherence in intensity evolution contains meaningful information, but that requiring directional agreement across multiple temporal scales sharpens the identification of storms with elevated conditional RI occurrence. This suggests that cross-scale agreement contributes additional occupancy stratification relative to single-window persistence alone while holding the persistence definition constant.

---

6. Discussion

The principal result is that sustained cross-scale alignment stratifies RI occurrence across the Atlantic record. The diagnostic identifies an enriched subset of storms but does not broadly classify all RI events. Its contribution is descriptive: temporal organization in best-track intensity evolution exhibits reproducible stratification behavior with distinct RI statistics. Era-stratified analyses indicate that the relationship is not confined to a single observing period, while upper-tail estimates remain sensitive to sample size and historical data quality. Comparisons with

single-window persistence metrics indicate that persistence in intensity evolution is itself informative. However, the multi-window diagnostic imposes a stricter operational definition of sustained directional alignment across smoothing windows. This stricter regime definition sharpens RI stratification at intermediate occupancy durations. The results support long-record robustness across observational eras, while remaining sensitive to known historical inhomogeneities.

The advisory-level and storm-level conditioning analyses evaluate different statistical formulations of the occupancy process. Advisory-level conditioning tests whether local occupancy behavior retains association with RI occurrence after inclusion of contemporaneous environmental covariates at individual advisory times. In contrast, storm-level formulations evaluate whether lifecycle-scale occupancy organization remains associated with storm-integrated RI realization. The substantial attenuation observed in the advisory-level conditioned specification therefore does not directly contradict the positive conditioned association observed in storm-level occupancy aggregates, because the two formulations operate on different aggregation configurations and dependence assumptions

These results should not be read as direct evidence of convective symmetry, vortex alignment, or inner-core structural evolution (Jiang 2012; Jiang and Ramirez 2013; Rogers et al. 2015; Miyamoto and Nolan 2018). The diagnostic is derived entirely from VMAX time series and cannot resolve those processes. A more appropriate interpretation is that best-track intensity evolution contains persistent temporal states associated with different RI outcomes. Future work can test whether these states align with independent structural observations from aircraft, microwave, radar, or satellite-derived fields.

Because the detector is constructed from temporally correlated intensity evolution, enrichment under autocorrelation-preserving nulls is expected. The analysis therefore tests whether timing and alignment remain separable under constrained replay. The primary contribution of the framework is therefore event-time occupancy characterization rather than operational RI prediction

The diagnostic differs from the RI definition because it does not require a fixed 24-h magnitude increase. Instead, it measures sustained directional agreement among causal smoothing representations of the intensity record. Environmental conditioning suggests that part of the occupancy–RI relationship overlaps with environmentally favorable periods of storm evolution. Because both quantities are derived from VMAX, the analysis evaluates stratification and non-equivalence rather than statistical independence. Attenuation under block shuffling indicates dependence on temporal ordering, consistent with the diagnostic capturing structured temporal evolution rather than marginal intensity properties alone.

Taken together, the results identify a reproducible long-record occupancy regime in best-track intensity evolution that stratifies RI occurrence.

---

7. Limitations

Several limitations should be noted:

- The diagnostic is derived solely from best-track VMAX and does not directly observe storm structure, environmental forcing, or physical mechanism.
- RI labels and the occupancy diagnostic are both derived from intensity evolution; the analysis evaluates stratification beyond simpler baselines, not full independence from intensity.
- The highest-occupancy subsets contain relatively few storms and should be interpreted as exploratory upper-tail regimes.
- HURDAT2 contains known inhomogeneities across observing eras, especially before the aircraft and satellite eras.
- Storm-level summaries reduce pseudo-replication but do not eliminate all temporal dependence; timing analyses require explicit occupancy-process or survival-style treatment.
- The multi-window alignment detector contains tunable construction choices, although sensitivity analyses indicate that the primary occupancy–RI relationship is stable across broad parameter neighborhoods.

- Additional work is needed to further evaluate environmental conditioning, basin transfer, independent structural observations, and survival/hazard behavior.
- The framework does not establish causal independence from intensity dynamics or evidence of a separate physical forcing process.

---

8. Conclusion

A causal temporal-coherence occupancy diagnostic derived from best-track intensity evolution identifies reproducible alignment regimes in Atlantic tropical cyclones over 1851–2024. Longer active occupancy is associated with elevated conditional RI occurrence, although upper-tail estimates remain sample-limited.

The results provide evidence that persistent cross-timescale alignment behaves as a measurable long-record feature associated with redistributed RI occupancy. This provides a foundation for future work using survival-style timing analysis, environmental conditioning, independent basin replication, and c comparison with independent structural diagnostics.

---

9. Data Availability

The Atlantic hurricane database (HURDAT2) used in this study is publicly available from the National Hurricane Center (https://www.nhc.noaa.gov/data/). Code and derived data supporting the temporal-coherence diagnostic are archived at Zenodo (DOI: https://zenodo.org/records/20242605). The repository includes a minimal, reproducible implementation of the diagnostic and example datasets sufficient to reproduce the analysis from HURDAT2.

---

10. Reproducibility and governance

All framework computations were performed sequentially in time using only current and prior observations. Detector construction, parameter declaration, and validation analyses were executed under frozen replay conditions with predeclared thresholds and forward-only

572 governance constraints. Validation outputs included parameter manifests, audit receipts, and
573 reproducibility artifacts associated with the frozen Atlantic structural replay archive (Peng 2011;
574 Nosek et al. 2018).
575
576 **11. Acknowledgements**
577
578 The author thanks Dr. John Kaplan (NOAA/AOML) for helpful discussions regarding rapid
579 intensification, persistence diagnostics, and environmental conditioning frameworks.
580 The author thanks the developers and maintainers of the HURDAT2 dataset and the broader
581 tropical cyclone research community for maintaining the historical record used in this analysis.
582 Large language models were used for editorial assistance and language refinement during
583 manuscript preparation. All scientific content, analysis, and interpretation is the responsibility of
584 the author.
585 This work received no external funding.
586 The author declares no conflicts of interest.
587
588 **12. References**
589
590 Allison, P. D., 1982: Discrete-time methods for the analysis of event histories. *Sociological*
591 *Methodology*, **13**, 61–98, https://doi.org/10.2307/270718
592 Andersen, P. K., and R. D. Gill, 1982: Cox's regression model for counting processes: A large
593 sample study. *Annals of Statistics*, **10**, 1100–1120, https://doi.org/10.1214/aos/1176345976
594 Cox, D. R., 1972: Regression models and life-tables. *Journal of the Royal Statistical Society:*
595 *Series B (Methodological)*, **34**, 187–202, https://doi.org/10.1111/j.2517-6161.1972.tb00899.x
596 Dawid, A. P., 1984: Present position and potential developments: Some personal views—
597 Statistical theory: The prequential approach. *Journal of the Royal Statistical Society: Series A*,
598 **147**, 278–292, https://doi.org/10.2307/2981683
599 DeMaria, M., Franklin, J. L., Onderlinde, M. J., and Kaplan, J., 2021: Operational forecasting of
600 tropical cyclone rapid intensification at the National Hurricane Center. *Atmosphere*, **12**, 683.
601 https://doi.org/10.3390/atmos12060683

602 Efron, B., 1979: Bootstrap methods: Another look at the jackknife. *Annals of Statistics*, **7**, 1–26,
603 https://doi.org/10.1214/aos/1176344552
604 Efron, B., 1986: Why isn't everyone a Bayesian? *The American Statistician*, **40**, 1–11,
605 https://doi.org/10.1080/00031305.1986.10475342
606 Jiang, H., 2012: The relationship between tropical cyclone intensity change and the strength of
607 inner-core convection. *Monthly Weather Review*, **140**, 1164–1176.
608 https://doi.org/10.1175/MWR-D-11-00134.1
609 Jiang, H., and Ramirez, E. M., 2013: Necessary conditions for tropical cyclone rapid
610 intensification as derived from 11 years of TRMM data. *Journal of Climate*, **26**, 6459–6470.
611 https://doi.org/10.1175/JCLI-D-12-00432.1
612 Kaplan, E. L., and P. Meier, 1958: Nonparametric estimation from incomplete observations.
613 *Journal of the American Statistical Association*, **53**, 457–481,
614 https://doi.org/10.1080/01621459.1958.10501452
615 Kaplan, J., and DeMaria, M., 2003: Large-scale characteristics of rapidly intensifying tropical
616 cyclones in the North Atlantic basin. *Weather and Forecasting*, **18**, 1093–1108.
617 https://doi.org/10.1175/1520-0434(2003)018<1093:LCORIT>2.0.CO;2
618 Kaplan, J., DeMaria, M., and Knaff, J. A., 2010: A revised tropical cyclone rapid intensification
619 index for the Atlantic and eastern North Pacific basins. *Weather and Forecasting*, **25**, 220–241.
620 https://doi.org/10.1175/2009WAF2222280.1
621 Kieper, M. E., and Jiang, H., 2012: Predicting tropical cyclone rapid intensification using the 37-
622 GHz ring pattern identified from passive microwave measurements. *Geophysical Research*
623 *Letters*, **39**, L13804. https://doi.org/10.1029/2012GL052115
624 Künsch, H. R., 1989: The jackknife and the bootstrap for general stationary observations. *Annals*
625 *of Statistics*, **17**, 1217–1241, https://doi.org/10.1214/aos/1176347265
626 Landsea, C. W., and Franklin, J. L., 2013: Atlantic hurricane database uncertainty and
627 presentation of a new database format. *Monthly Weather Review*, **141**, 3576–3592.
628 https://doi.org/10.1175/MWR-D-12-00254.1
629 Landsea, C. W., Franklin, J. L., and Beven, J. L., II, 2022: The revised Atlantic hurricane
630 database (HURDAT2): Documentation and format updates. National Hurricane Center, NOAA.
631 https://www.nhc.noaa.gov/data/

Liang, K.-Y., and S. L. Zeger, 1986: Longitudinal data analysis using generalized linear models. *Biometrika*, **73**, 13–22, https://doi.org/10.1093/biomet/73.1.13

Lin, D. Y., and L. J. Wei, 1989: The robust inference for the Cox proportional hazards model. *Journal of the American Statistical Association*, **84**, 1074–1078, https://doi.org/10.1080/01621459.1989.10478874

Miyamoto, Y., and Nolan, D. S., 2018: Structural changes preceding rapid intensification in tropical cyclones as shown in a large ensemble of idealized simulations. *Journal of the Atmospheric Sciences*, **75**, 555–569. https://doi.org/10.1175/JAS-D-17-0177.1

Nosek, B. A., et al., 2018: The preregistration revolution. *Proceedings of the National Academy of Sciences*, **115**, 2600–2606, https://doi.org/10.1073/pnas.1708274114

Ng, E. K. W., and Chan, J. C. L., 2012: Geophysical applications of partial wavelet coherence and multiple wavelet coherence. *Journal of Atmospheric and Oceanic Technology*, **29**, 1845–1853. https://doi.org/10.1175/JTECH-D-12-00056.1

Peng, R. D., 2011: Reproducible research in computational science. *Science*, **334**, 1226–1227, https://doi.org/10.1126/science.1213847

Politis, D. N., and J. P. Romano, 1994: The stationary bootstrap. *Journal of the American Statistical Association*, **89**, 1303–1313, https://doi.org/10.1080/01621459.1994.10476870

Rogers, R. F., Reasor, P. D., and Zhang, J. A., 2015: Multiscale structure and evolution of Hurricane Earl (2010) during rapid intensification as sampled by aircraft. *Monthly Weather Review*, **143**, 536–562. https://doi.org/10.1175/MWR-D-14-00175.1

Shi, D., Chen, G., and Xie, X., 2023: Revisiting the relationship between tropical cyclone rapid intensification and the distribution of inner-core precipitation. *Geophysical Research Letters*, **50**, e2023GL104810. https://doi.org/10.1029/2023GL104810

Tashman, L. J., 2000: Out-of-sample tests of forecasting accuracy: An analysis and review. *International Journal of Forecasting*, **16**, 437–450, https://doi.org/10.1016/S0169-2070(00)00065-0

Theiler, J., S. Eubank, A. Longtin, B. Galdrikian, and J. D. Farmer, 1992: Testing for nonlinearity in time series: The method of surrogate data. *Physica D*, **58**, 77–94, https://doi.org/10.1016/0167-2789(92)90102-S

Torrence, C., and Compo, G. P., 1998: A practical guide to wavelet analysis. *Bulletin of the American Meteorological Society*, **79**, 61–78. https://doi.org/10.1175/1520-0477(1998)079<0061:APGTWA>2.0.CO;2

Vecchi, G. A., and Knutson, T. R., 2008: On estimates of historical North Atlantic tropical cyclone activity. *Journal of Climate*, **21**, 3580–3600. https://doi.org/10.1175/2008JCLI2178.1

Vecchi, G. A., and Knutson, T. R., 2011: Estimating annual numbers of Atlantic hurricanes missing from the HURDAT database (1878–1965) using ship track density. *Journal of Climate*, **24**, 1736–1746. https://doi.org/10.1175/2010JCLI3810.1

Vecchi, G. A., Delworth, T., Gudgel, R., Kapnick, S., Rosati, A., Wittenberg, A., Zeng, F., Anderson, W., Balaji, V., Dixon, K., et al., 2021: Tropical cyclone sensitivities to CO_2 doubling: Roles of atmospheric resolution, synoptic variability, and background climate changes. *Climate Dynamics*, **57**, 1965–1986. https://doi.org/10.1007/s00382-021-05867-2